4480 *Chem. Mater.* **2009,** *21,* 4480–4489
DOI:10.1021/cm901219u

CHEMISTRY OF MATERIALS
Article

Magnetism and Negative Magnetoresistance of Two Magnetically Ordering, Rare-Earth-Containing Zintl phases with a New Structure Type: $EuGa_2Pn_2$ (Pn = P, As)

Andrea M. Goforth,[†,§] Håkon Hope,[†] Cathie L. Condron,[†] Susan M. Kauzlarich,*[,†] Newell Jensen,[‡] Peter Klavins,[‡] Samuel MaQuilon,[‡] and Zachary Fisk[‡,⊥]

[†]*Department of Chemistry and* [‡]*Department of Physics, University of California, One Shields Avenue, Davis, California 95616.* [§]*Current address: Department of Chemistry, Portland State University, 1719 SW 10th Avenue, Portland, OR 97201.* [⊥]*Current address: Department of Physics, University of California, Irvine, CA 92697.*

Received May 4, 2009. Revised Manuscript Received July 24, 2009

Single crystals of $EuGa_2Pn_2$ (Pn = P, As) were grown from a molten Ga flux and characterized by single-crystal X-ray diffraction at 100(1) K. They are isostructural and crystallize in a new structure type (monoclinic, $P2/m$, a = 9.2822(9) Å, b = 3.8967(4) Å, c = 12.0777(11) Å, β = 95.5220(10)°, R1 = 0.0148, wR2 = 0.0325 ($EuGa_2P_2$) and a = 9.4953(7) Å, b = 4.0294(3) Å, c = 12.4237(9) Å, β = 95.3040(10)°, R1 = 0.0155, wR2 = 0.0315 ($EuGa_2As_2$)). The structures consist of alternating layers of two-dimensional Ga_2Pn_2 anions and Eu cations. The anion layers are composed of Ga_2Pn_6 staggered, ethane-like moieties having a rare Ga−Ga bonding motif; these moieties are connected in a complex fashion by means of shared Pn atoms. Both structures show small residual electron densities that can be modeled by adding a Eu atom and removing two bonded Ga atoms, resulting in structures (< 2%) where most of the atoms are the same, but there is a difference in bonding that leads to one-dimensional ribbons of parallel Ga_2Pn_6 staggered, ethane-like moieties. The compounds can be understood within the Zintl formalism, but show metallic resistivity. Magnetization measurements performed on single crystals show low-temperature magnetic anisotropy as well as multiple magnetic ordering events that occur at and below 24 and 20 K for the phosphorus and arsenic analogs, respectively. The magnetic coupling between Eu ions is attributed to indirect exchange via an RKKY interaction, which is consistent with the metallic behavior. The compounds display large negative magnetoresistance of up to −80 and −30% (MR = $[(\rho(H)-\rho(0))/\rho(H)] \times 100\%$) for Pn = P, As, respectively, which is maximal at the magnetic ordering temperatures in the highest measured field (5T).

Introduction

Zintl phases are defined as valence-precise compounds of the heavier main group elements where there is complete charge transfer from highly electropositive elements, generally Group 1 or 2 metals, to more electronegative main group elements, generally from Groups 13−15.[1−3] Resulting from the myriad ways in which these elements can fill their valence, through ionic bonding, homo- or heteroatomic covalent bonding, lone pairs, etc., Zintl phases exhibit significant structural diversity. Thus, a very large number of examples of Zintl phases containing homo- or heteropolyanions (1-, 2-, or 3-dimensional), as well as discrete anions (0-dimensional), have been synthesized and structurally characterized. In the preparation of these compounds, the outcome depends on many factors, such as the elements involved (relative electronegativities, sizes), the stoichiometry and concentration of reagents, and the reaction temperature and event profile (which provide some degree of both thermodynamic and kinetic control over product identity/distribution).[4−8] Thus, by careful consideration of the reaction parameters, the potential for structural diversity leads to endless imaginable compositions and structure types that adhere to the original Zintl formalism. This formalism has since been expanded to include transition- or rare-earth metal analogues of main group phases.[9,10]

*Corresponding author. E-mail: smkauzlarich@ucdavis.edu.

(1) Müller, U. Polyanionic and polycationic compounds. Zintl phases. In *Inorganic Structural Chemistry*; Meyer, G., Nakamura, A., Eds.; John Wiley & Sons: Chichester, U.K., 1991; pp 116−138.
(2) Kauzlarich, S. M. *Chemistry, Structure and Bonding of Zintl Phases and Ions: Selected Topics and Recent Advances*; VCH Publishers: New York, 1996; p 306.
(3) Corbett, J. D. *Angew. Chem., Int. Ed.* **2000**, *39*, 670.
(4) Kanatzidis, M. G.; Pöttgen, R.; Jeitschko, W. *Angew. Chem., Int. Ed.* **2005**, *44*, 6996.
(5) Canfield, P. C.; Fisk, Z. *Philos. Mag. B* **1992**, *65*, 1117.
(6) Payne, A. C.; Spauvre, A. E.; Olmstead, M. M.; Kauzlarich, S. M.; Chan, J. Y.; Reisner, B. A.; Lynn, J. W. *J. Solid State Chem.* **2002**, *163*, 498.
(7) Payne, A. C.; Spauvre, A. E.; Holm, A. P.; Olmstead, M. M.; Kauzlarich, S. M.; Klavins, P. *J. Alloys Compd.* **2002**, *338*, 229.
(8) Jiang, J.; Kauzlarich, S. M. *Chem. Mater.* **2006**, *18*, 435.
(9) Kauzlarich, S. M.; Chan, J. Y.; Taylor, B. R. Exploitation of Zintl Phases in the Pursuit of Novel Magnetic and Electronic Materials. In *Inorganic Materials Synthesis*; Winter, C. H., Hoffman, D. M., Eds.; American Chemical Society: Washington, D.C., 1999; pp 15−27.
(10) Kauzlarich, S. M.; Payne, A. C.; Webb, D. J. *Magnetism and Magnetotransport Properties of Transition Metal Zintl Isotypes. In Magnetism: Molecules to Materials III*; Miller, J. S., Drillon, M., Eds.; Wiley-VCH: Weinheim, Germany, 2002; pp 37−62.

 Published on Web 08/28/2009

It should be noted that the specific combinations of structural features observed in traditional Zintl phases are often responsible for their useful materials properties. These features include closed-shell electron configurations, propensity to form catenated structures, large unit cells, structural complexity, and topological variety, as well as heavy-element compositions. Recently, Zintl phases have been recognized as a new class of important materials for thermoelectric applications, where the efficiency of thermal and electrical conductivity relies simultaneously on many of the aforementioned structural features.[11−13]

Rare-earth analogues of alkali or alkaline-earth Zintl phases achieve the same complexity and variety as their main-group counterparts, but the replacement of magnetically inert cations with potentially high magnetic moment metal cations can lead to interesting magnetic ordering or magneto-electronic properties in these phases in addition to the more traditional properties. Magnetoresistance (MR) has been observed in several rare-earth Zintl analogues.[6,8−10,14−17] It is thought that the MR behavior of rare-earth-containing Zintl phases originates from interactions between the localized magnetic moment on the rare-earth cations and the delocalized conduction electrons of the Zintl polyanions. Such materials could be useful in magnetic storage applications. Additionally, magnetic coupling interactions, such as ferromagnetism and antiferromagnetism, frequently occur in these compounds, even though the magnetic cations are often separated by large distances. These magnetic ordering interactions are often anisotropic with respect to crystal structure and material orientation, leading to deductions about magnetocrystalline structure as well as to crystal structure/magnetic property correlations.[6,8−14] Correlated measurements of resistivity, magnetic anisotropy, and structure are aided by the ability to grow large, high-quality single crystals of Zintl phases by employing a high-temperature flux growth method, with slow cooling to promote growth of larger crystals and centrifugation to remove the molten flux above its melting point. The use of both reactive (incorporated in product) and nonreactive (not incorporated in product) fluxes as a technique for synthesizing large, high-quality single crystals has been reviewed in the literature.[4,5]

Exploration of the ternary A−Ga−Pn phase diagrams (A = electropositive element, Pn = pnicogen) using a reactive Ga flux may reveal new structure types that are of particular interest because superconductivity, heavy fermion behavior, and magnetoresistance have been discovered in several different Zintl and intermetallic structure types. Many of these interesting properties are found in materials of composition AM_2X_2 (M = transition or main group element, X = Group 13−15 element), which is a particularly diverse structural class.[8,14,18−22] Recent discovery of colossal magnetoresistance (CMR) in several of the magnetically ordering AM_2X_2 compounds (e.g., $EuIn_2P_2$ and $EuIn_2As_2$),[8,14] provides incentive for additional research into these types of compounds in order to provide correlations between material composition, structure, and the observed electrical, magnetic, and/or magneto-electronic properties.

Here we present two new, europium-containing Zintl phases of stoichiometry $EuGa_2Pn_2$ (Pn = P, As). These two compounds exhibit an unusual and novel structure type for intermetallic compounds with stoichiometry AM_2X_2, as well as large negative magnetoresistance. For these phases, there are currently no known main group analogues. The magnetic and charge-transport properties of these low-symmetry, monoclinic $EuGa_2Pn_2$ phases are compared to their hexagonally symmetric indium analogues, $EuIn_2Pn_2$ (Pn = P, As),[8,14] as well as to other metallic magnetoresistive compounds. Trends in the effects of element composition and crystal structure on the observed magnetoresistance are discussed.

Experimental Section

Materials. All reagents were handled under an inert atmosphere, either N_2 or Ar. Eu ribbon (3 mm, 99.999%, Ames Lab) was first brushed to remove the oxidized layer and then cut into small pieces. Crushed elemental As (polycrystalline lump, 99.9999+% puratronic, J. Matthey), Ga (6 mm pellets, 99.9999%, Alfa Aesar), and red phosphorus (polycrystalline lump, 99.9999+% puratronic, J. Matthey) were used as received.

Synthesis. $EuGa_2P_2$ was synthesized using a 3:150:6 (Eu:Ga:P) molar ratio of the elements (11 g total wt.). In this reaction, Ga is both a reactant and a flux. The elements were loaded into a 5 mL alumina crucible in the order: Ga, Eu and P, Ga. The crucible, held in place between two layers of tightly packed quartz wool, was subsequently sealed under ~1/5 atm Ar in a fused silica ampule. The reaction vessel was then heated in a box furnace in an upright position. The reaction contents were heated to 1100 °C, kept at this temperature for 16 h, cooled to 600 °C at 2 °C/h, and finally centrifuged to remove molten flux at 600 °C. The ampule was broken in air to reveal large, silver parallelpipeds of $EuGa_2P_2$ as the sole reaction product.

$EuGa_2As_2$ was synthesized in an analogous procedure from a reactive Ga flux, with a 3:51:6 (Eu:Ga:As) molar ratio of the elements (10 g total weight). The sealed ampule was heated at a rate of 60 °C/h to 1100 °C and maintained at this temperature for 6 h before it was cooled, at a rate of 200 °C/h, to 850 °C. The reaction vessel was maintained at 850 °C for 6 h before it was slow-cooled, at a rate of 1 °C/h, to 500 °C, at which point it was

(11) Kauzlarich, S. M.; Brown, S. R.; Snyder, G. J. *Dalton Trans.* **2007**, *21*, 2099.
(12) Brown, S. R.; Kauzlarich, S. M.; Gascoin, F.; Snyder, G. J. *Chem. Mater.* **2006**, *18*, 1873.
(13) Kanatzidis, M. G. *Chem. Mater.* **1999**, *11*, 3154.
(14) Goforth, A. M.; Klavins, P.; Fettinger, J. C.; Kauzlarich, S. M. *Inorg. Chem.* **2008**, *47*, 11048.
(15) Payne, A. C.; Olmstead, M. M.; Kauzlarich, S. M.; Webb, D. J. *Chem. Mater.* **2001**, *13*, 1398.
(16) Chan, J. Y.; Kauzlarich, S. M.; Klavins, P.; Shelton, R. N.; Webb, D. J. *Chem. Mater.* **1997**, *9*, 3132.
(17) Jiang, J.; Olmstead, M. M.; Kauzlarich, S. M.; Lee, H.-O.; Klavins, P.; Fisk, Z. *Inorg. Chem.* **2005**, *44*, 5322.
(18) Braun, H. F.; Engel, N.; Parthé, E. *Phys. Rev. B* **1983**, *28*, 1389.
(19) Ronning, F.; Klimczuk, T.; Bauer, E. D.; Volz, H.; Thompson, J. D. *J. Phys.−Condens. Mater.* **2008**, *20*, 322201.
(20) Steglich, F.; Ahlheim, U.; Franse, J. J. M.; Grewe, N.; Rainer, D.; Rauchschwalbe, U. *J. Magn. Magn. Mater.* **1985**, *52*, 54.
(21) Steglich, F.; Aarts, J.; Bredl, C. D.; Lieke, W.; Meschede, D.; Franz, W.; Schäfer, H. *Phys. Rev. Lett.* **1979**, *43*, 1892.
(22) Jeitschko, W.; Glaum, R.; Boonk, L. *J. Solid State Chem.* **1987**, *69*, 93.

Table 1. Crystal Data and Structure Refinement for $EuGa_2Pn_2$ (Pn = P, As) at 100 (1) K

	$EuGa_2P_2$	$EuGa_2As_2$
space group	*P*2/*m*	*P*2/*m*
a (Å)	9.2822(9)	9.4953(7)
b (Å)	3.8967(4)	4.0294(3)
c (Å)	12.0777(11)	12.4237(9)
β (deg)	95.5220(10)	95.3040(10)
V (Å^3)	434.82(7)	473.30(6)
Z	4	4
density (calcd) (Mg/m^3)	5.398	6.192
absorp coeff (mm^{-1})	27.064	38.065
theta range (deg)	2.65−27.48	2.59−27.48
no. of reflns collected	6586	6040
no. of independent reflns	1134	1240
data/restraints/parameters	1134/0/66	1240/0/66
GOF on F^2	1.197	1.261
final R indices [$I > 2\sigma(I)$][a]	R1 = 0.0148	R1 = 0.0155
	wR2 = 0.0325	wR2 = 0.0315
R indices (all data)	R1 = 0.0159	R1 = 0.0161
	wR2 = 0.0327	wR2 = 0.0317
largest diff. peak and hole (e Å^{-3})	1.14 and −0.84	1.74 and −0.90

[a] $R1 = [\Sigma||F_o| - |F_c||]/\Sigma|F_o|$; $wR2 = \{[\Sigma w[(F_o)^2 - (F_c)^2]^2]\}^{1/2}$; $wR2 = [\sigma^2(F_o) + (0.0471P)^2 + (0.5945P)]$, where $P = [\max(F_o^2, 0) + 2F_c^2/3]$.

removed from the furnace, inverted, and centrifuged to remove the flux. The vessel was subsequently broken in air to reveal large, silver parallelepipeds of $EuGa_2As_2$ as the sole crystalline product.

Crystal Structure Determination. X-ray intensity data were collected on suitable single crystals of $EuGa_2Pn_2$ (Pn = P, As) at 100(1) K using a Bruker SMART APEXII CCD-based diffractometer (Mo Kα radiation, $\lambda = 0.71073$ Å).[23] Raw data frame integration and Lorentz and polarization corrections were performed using the SAINT+ program.[23] The data were corrected for absorption effects based on fitting a function to the empirical transmission surface, as sampled by multiple equivalent reflections with the program SADABS.[23] Direct methods structure solution and full-matrix least-squares refinement against F^2 were performed with SHELX.[24] X-ray data collection and structure refinement details for the compounds are listed in Table 1.

$EuGa_2P_2$ and $EuGa_2As_2$ crystallize in primitive, monoclinic unit cells. There are no systematic reflection absences. This presents a choice of the three space groups *P*2, *Pm*, and *P*2/*m*. The structures were successfully solved and refined with *P*2/*m*. All atoms were refined with anisotropic atomic displacement parameters. For both $EuGa_2P_2$ and $EuGa_2As_2$, significant residual electron density (approximately 4 e Å^{-3}) remained after refinement. To rule out the possibility that this was sample specific, we collected additional data sets from different crystals. The residual density is a property of all measured crystals.

The residual electron density in both structures is located at corresponding crystallographic sites, at the midpoint of the Ga(2)−Ga(3) bond. Inclusion of the residual peak as a partial Eu atom led to a drop in R from 0.020 to 0.015 for the phosphide analog, so it is clearly part of the structure. The location of an extra Eu atom in the center of the Ga−Ga bond requires the removal of the corresponding Ga atoms. This was expected to be discernible from refined Ga occupancies. The occupancies of the relevant atoms were first individually refined. For the P compound, the occupancy of the partial Eu atom refined to 1.8%, and the occupancies of each of the partially displaced Ga atoms refined to 98.2%, all with small uncertainties. Occupancies of other Ga atoms refined to 100%, within narrow uncertainties. In the final refinements the occupancies were coupled to refine as one single variable, again leading to a substitution of 1.8%. This substitution by Eu for a pair of Ga atoms in the major structure ($EuGa_2P_2$) leads to a new structure with crystallographic composition $Eu_3Ga_2P_4$. A corresponding treatment of the $EuGa_2As_2$ data indicates a 1.4% substitution by Eu to give the $Eu_3Ga_2As_4$ structure. Other refinement models where the residual density was assigned to either Ga or Pn did not provide reasonable bond distances and angles. However, with Eu as the substituting atom, the bond distances (Eu−Pn) and angles (Pn−Eu−Pn) for the Eu(4P) atoms are comparable to those observed in the unambiguous $EuPn_6$ polyhedra (see Table 3), further supporting this assignment.

X-ray Powder Diffraction. Representative samples from each reaction were ground to fine powders in air using an agate mortar and pestle. Powder diffraction patterns were collected in air on an INEL diffractometer (Co Kα radiation, $\lambda = 1.78890$ Å) and compared with diffraction patterns calculated from the single-crystal structural parameters, using the program CrystalDiffract.[25] PXRD was used to qualitatively identify the phases present upon completion of each flux reaction, and conditions were identified that produced each compound as a pure phase.

Magnetic Measurements. Magnetic measurements were made on single crystals (weighing 0.69 mg, $EuGa_2P_2$; or 0.87 − 2.45 mg, $EuGa_2As_2$) whose identities were verified by single-crystal X-ray diffraction prior to measurement. Crystallographic orientations were not verified prior to measurement because of low crystal symmetry (monoclinic) and anisotropic crystal habits. The crystals were mounted individually, with their long needle axes either parallel or perpendicular to the applied magnetic field. In both phases the long needle axis coincides with the crystallographic *b*-axis. For both the perpendicular and the parallel orientations, the crystals were mounted on thin Mylar strips and covered with Kapton tape. This method of sample preparation provides a negligible signal from the sample holder, so the data were not corrected. The samples were then mounted in drinking straws, and magnetization versus temperature (ZFC/FC sequences, 2−320/280−2 K) measurements were recorded in applied fields of 0.01, 0.1, and 1 T using a Quantum Design MPMS superconducting quantum interference device (SQUID magnetometer). Magnetization versus field measurements (−5 T to 5 T) were also recorded in both orientations for the samples at $T = 5$ K.

Transport Properties. Electrical transport measurements were made with four platinum leads attached along the needle axis (*b*-axis) of $EuGa_2P_2$ and $EuGa_2As_2$ with silver paint (approximate crystal dimensions for both were $2 \times 2 \times 3$ mm^3). In light of the complicated magnetization versus temperature and magnetization versus field data collected in the experiments above (described in the Results section, vide infra), only one orientation of crystals, with their *b*-axes coincident with H, was measured. Several different crystals of each phase were measured and provided consistent results. A Keithley model 224 current source and model 181 voltmeter were interfaced to the SQUID magnetometer for the measurements. A constant current (I) of 1 mA was applied along the *b*-axis through the two outer leads. The voltage drop (V) between the two innermost electrical contacts was measured. The data followed Ohm's Law, $V = IR$ (R = resistance). Resistivity, ρ, was determined at each temperature by means of the equation $\rho = RA/l$, where

(23) *SMART, SAINT+, and SADABS*; Bruker AXS: Madison, WI, 1998.
(24) Sheldrick, G. M. *SHELXL-97*; Bruker AXS: Madison, WI, 1997.
(25) *CrystalDiffract*; CrystalMaker Software Limited: Oxfordshire, U.K., 2006.

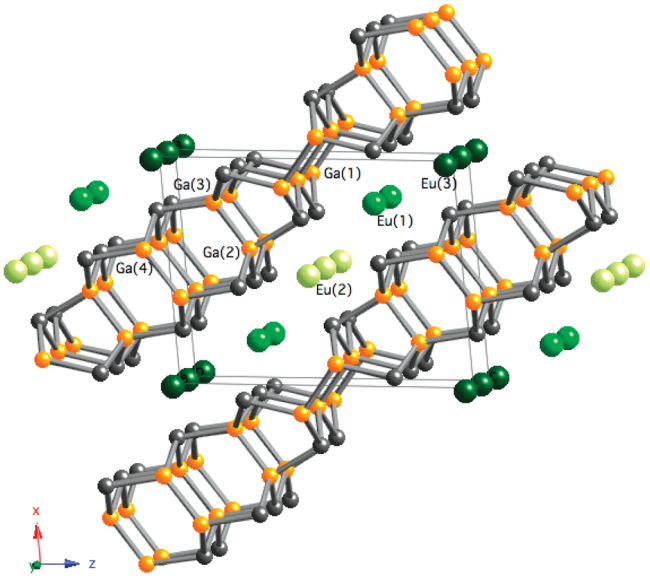

Figure 1. [010] view of the structure of $EuGa_2As_2$ ($EuGa_2P_2$ is isostructural) showing the anionic layers with Eu cations. The crystallographic sites are labeled. Eu, Ga, and As atoms are indicated by green, gold, and gray spheres, respectively. Crystallographically distinct Eu cations are differentiated with different shades of green.

A = cross-sectional area and l = length between the innermost silver paint contacts of the voltage leads. Resistivity as a function of temperature at several applied fields, ranging from 0 to 5 T, was measured for each of the samples.

Results and Discussion

Crystal Structures. The most commonly observed structure types for compounds of the composition AM_2X_2 (A = electropositive element, M = transition or main group metal, and X = element from Group 13, 14 or 15) are the tetragonal $ThCr_2Si_2$ ($I4/mmm$), closely related $CaBe_2Ge_2$ (tetragonal, $P4/nmm$), and trigonal $CaAl_2Si_2$ ($P\bar{3}m1$) structure types.[18,22,26−29] AM_2X_2 phases can theoretically achieve a remarkable structural diversity, depending on factors such as the relative sizes and coordination preferences of the large number of elements that can be accommodated, and by taking advantage of the variable connectivity possible for main group polyanions. Thus, our group has recently reported the synthesis and structural characterization of hexagonal $EuIn_2Pn_2$ compounds (Pn = P, As; $P6_3/mmc$),[8,14] which display structural similarities to the three common AM_2X_2 structure types. The $ThCr_2Si_2$, $CaBe_2Ge_2$, $CaAl_2Si_2$, and $EuIn_2Pn_2$ structure types all consist of $[M_2X_2]^{n-}$ anionic layers, which alternate with cation layers along one crystallographic direction. The coordination environments and bonding arrangements within the M−X layers vary between the structures, as do the space group symmetries.

Table 2. Atomic Coordinates and Equivalent Isotropic Displacement Parameters (U_{eq})[a] for $EuGa_2Pn_2$ (Pn = P, As)

atom	x	y	z	U_{eq} (Å^2)	occ.
			$EuGa_2P_2$		
Eu(1)	0.19443(2)	0.0000	0.279942(18)	0.00795(7)	1
Eu(2)	0.5000	0.5000	0.5000	0.00703(8)	1
Eu(3)	0.0000	0.5000	0.0000	0.00688(8)	1
Ga(1)	−0.11199(5)	0.5000	0.43422(4)	0.00695(10)	1
Ga(2)	0.59696(5)	0.0000	0.27925(4)	0.00697(11)	0.9820(6)
Ga(3)	−0.19756(5)	0.0000	0.17222(4)	0.00710(11)	0.9820(6)
Ga(4)	0.39558(5)	0.5000	0.05613(4)	0.00713(10)	1
P(1)	−0.05576(12)	0.5000	0.23984(9)	0.0072(2)	1
P(2)	0.44202(12)	0.5000	0.25642(9)	0.0070(2)	1
P(3)	0.26386(12)	0.0000	0.53723(9)	0.0075(2)	1
P(4)	0.23966(12)	0.0000	0.02717(9)	0.0074(2)	1
Eu(4P)[b]	−0.3050(12)	0.0000	0.2194(10)	0.008	0.0180(6)
			$EuGa_2As_2$		
Eu(1)	0.20004(2)	0.0000	0.276540(18)	0.00673(7)	1
Eu(2)	0.5000	0.5000	0.5000	0.00580(8)	1
Eu(3)	0.0000	0.5000	0.0000	0.00583(8)	1
Ga(1)	−0.10862(5)	0.5000	0.43691(4)	0.00591(11)	1
Ga(2)	0.60436(5)	0.0000	0.28102(4)	0.00580(11)	0.9863(7)
Ga(3)	−0.19480(5)	0.0000	0.17527(4)	0.00597(11)	0.9863(7)
Ga(4)	0.39829(5)	0.5000	0.05440(4)	0.00600(11)	1
As(1)	−0.04984(5)	0.5000	0.24166(4)	0.00542(10)	1
As(2)	0.44668(5)	0.5000	0.25577(4)	0.00536(10)	1
As(3)	0.26186(5)	0.0000	0.53228(4)	0.00550(10)	1
As(4)	0.24058(5)	0.0000	0.02570(4)	0.00530(10)	1
Eu(4P)[b]	−0.2959(18)	0.0000	0.2236(14)	0.007	0.0137(7)

[a] U_{eq} is defined as one-third of the trace of the orthogonalized U^{ij} tensor. [b] The Eu(4P) displacement parameter was refined isotropically.

Structural diversity in the AM_2X_2 structure type is further exemplified by the two new compounds reported herein, $EuGa_2P_2$ and $EuGa_2As_2$, which crystallize in an unprecedented, monoclinic structure type that is related to the layered, hexagonal $EuIn_2Pn_2$ phases. The anionic $[Ga_2Pn_2]^{2-}$ unit of $EuGa_2Pn_2$ may be considered to be a structural variant of the $[In_2Pn_2]^{2-}$ anionic unit of $EuIn_2Pn_2$ in terms of the connectivity of M_2Pn_6 ethane-like moieties. The structures further differ in the number of crystallographically distinct europium atoms, which reside between the anion layers in both structures, with only one Eu site in the indium compounds as opposed to three in the lower symmetry gallium analogues.[8,14] A view of the structure of $EuGa_2Pn_2$ is shown in Figure 1. Tables 2 and 3 provide positional parameters and selected distances and angles. The local coordination environments are tetrahedral Ga and pyramidal P or As. The Ga atoms are found in connected pairs, with each Ga additionally bonded to three Pn, forming an ethane-like moiety in a staggered conformation. In contrast, in $EuIn_2Pn_2$, the In_2Pn_6 moiety is found in an eclipsed conformation, which establishes the hexagonal symmetry. A similarly staggered, ethane-like moiety, Ga_2Sb_6, is observed in $BaGa_2Sb_2$,[30] which displays yet another AM_2X_2 structure type in which the M_2Pn_6 units are connected into a 3D anionic framework. In $EuGa_2Pn_2$ the connectivity of the staggered moiety results in a two-dimensional layered structure, with layers of Eu^{2+} between the $[Ga_2Pn_2]^{2-}$ layers, rather than in a three-dimensional network with cations in cavities.

(26) Grytsiv, A.; Kaczorowski, D.; Leithe-Jasper, A.; Rogl, P.; Godart, C.; Potel, M.; Noël, H. *J. Solid State Chem.* **2002**, *163*, 37.
(27) Bobev, S.; Merz, J.; Lima, A.; Firtsch, V.; Thompson, J. D.; Sarrao, J. L.; Gillessen, M.; Dronskowski, R. *Inorg. Chem.* **2006**, *45*, 4047.
(28) Brock, S. L.; Greedan, J. E.; Kauzlarich, S. M. *J. Solid State Chem.* **1994**, *113*, 303.
(29) Hellmann, A.; Löhken, A.; Wurth, A.; Mewis, A. *Z. Naturforsch.* **2007**, *62b*, 155.
(30) Kim, S.-J.; Kanatzidis, M. G. *Inorg. Chem.* **2001**, *40*, 3781.

Table 3. Selected Interatomic Distances (Å) and Angles (deg) for $EuGa_2P_2$ and $EuGa_2As_2$

distances	$EuGa_2P_2$	$EuGa_2As_2$	distances	$EuGa_2P_2$	$EuGa_2As_2$
Eu(1)−Pn(1)	3.0344(9)	3.1123(4)	Eu(1)−Eu(1)	3.8967(4)	4.0294(3)
Eu(1)−Pn(2)	3.0470(9)	3.1180(4)	Eu(1)−Eu(3)	4.1606(3)	4.2737(3)
Eu(1)−Pn(3)	3.1122(12)	3.1772(6)	Eu(2)−Eu(2)	3.8967(4)	4.0294(3)
Eu(1)−Pn(4)	3.1214(11)	3.1751(5)	Eu(4P)−Eu(4P)	3.8967(4)	4.0294(3)
Eu(2)−Pn(2)	2.9393(11)	3.0296(5)	Ga(1)−Pn(1)	2.4535(12)	2.5388(7)
Eu(2)−Pn(3)	2.9987(8)	3.0823(4)	Ga(1)−Pn(3)	2.4486(7)	2.5349(4)
Eu(3)−Pn(4)	2.9516(8)	3.0405(4)	Ga(2)−Pn(2)	2.4216(7)	2.5124(4)
Eu(3)−Pn(1)	2.9912(11)	3.0823(5)	Ga(2)−Pn(3)	2.4558(13)	2.5395(7)
Eu(4P)−Pn(1)	3.016(9)	3.078(13)	Ga(3)−Pn(4)	2.4023(12)	2.4945(7)
Eu(4P)−Pn(2)	3.117(9)	3.220(14)	Ga(3)−Pn(1)	2.4471(8)	2.5346(4)
Eu(4P)−Pn(3)	2.927(12)	3.020(17)	Ga(4)−Pn(2)	2.4159(12)	2.5016(7)
Eu(4P)−Pn(4)	3.096(12)	3.190(17)	Ga(4)−Pn(4)	2.4322(7)	2.5159(4)
Ga(1)−Ga(1)	2.4922(9)	2.4728(10)	Ga(2)−Ga(3)	2.4048(6)	2.4137(7)
Ga(4)−Ga(4)	2.4703(9)	2.4578(10)			
angles	**$EuGa_2P_2$**	**$EuGa_2As_2$**	**angles**	**$EuGa_2P_2$**	**$EuGa_2As_2$**
Pn(1)−Eu(1)−Pn(1)	79.90(3)	80.683(13)	Pn(4)−Eu(3)−Pn(4)	82.61(3)	83.001(13)
Pn(1)−Eu(1)−Pn(2)	98.46(2)	97.988(10)	Pn(4)−Eu(3)−Pn(1)	84.77(3)	85.458(11)
Pn(2)−Eu(1)−Pn(2)	79.50(3)	80.505(13)	Pn(4)−Eu(3)−Pn(4)	97.39(3)	96.999(13)
Pn(1)−Eu(1)−Pn(4)	90.96(3)	91.339(12)	Pn(4)−Eu(3)−Pn(1)	95.23(3)	94.543(11)
Pn(2)−Eu(1)−Pn(4)	74.64(3)	76.035(11)	Pn(1)−Eu(3)−Pn(1)	180.0	180.0
Pn(1)−Eu(1)−Pn(3)	103.95(3)	101.960(12)	Pn(4)−Eu(3)−Pn(4)	180.0	180.0
Pn(2)−Eu(1)−Pn(3)	90.43(3)	90.687(12)	Pn(3)−Eu(4P)−Pn(1)	83.9(3)	85.2(4)
Pn(1)−Eu(1)−Pn(2)	165.52(3)	167.300(14)	Pn(1)−Eu(4P)−Pn(1)	80.5(3)	81.8(4)
Pn(3)−Eu(1)−Pn(4)	160.41(3)	162.466(14)	Pn(1)−Eu(4P)−Pn(4)	81.9(3)	83.0(4)
Pn(2)−Eu(2)−Pn(3)	85.18(3)	85.778(11)	Pn(3)−Eu(4P)−Pn(2)	83.3(3)	83.5(4)
Pn(3)−Eu(2)−Pn(3)	81.04(3)	81.633(13)	Pn(1)−Eu(4P)−Pn(2)	99.61(6)	99.28(7)
Pn(2)−Eu(2)−Pn(3)	94.82(3)	94.223(11)	Pn(2)−Eu(4P)−Pn(2)	77.4(3)	77.5(4)
Pn(3)−Eu(2)−Pn(3)	98.96(3)	98.367(13)	Pn(4)−Eu(4P)−Pn(2)	111.0(3)	108.4(4)
Pn(2)−Eu(2)−Pn(2)	180.0	180.0	Pn(3)−Eu(4P)−Pn(4)	161.3(4)	164.4(6)
Pn(3)−Eu(2)−Pn(3)	180.0	180.0	Pn(1)−Eu(4P)−Pn(2)	167.1(4)	168.6(6)
Pn(1)−Ga(1)−Pn(3)	108.25(3)	108.920(18)	Pn(3)−Ga(1)−Ga(1)	111.50(3)	111.17(2)
Pn(3)−Ga(1)−Pn(3)	105.44(4)	105.27(3)	Pn(1)−Ga(1)−Ga(1)	111.64(4)	111.19(3)
Pn(2)−Ga(2)−Pn(2)	107.14(5)	106.62(3)	Pn(2)−Ga(2)−Ga(3)	115.58(3)	115.071(18)
Pn(2)−Ga(2)−Pn(3)	110.97(3)	110.857(18)	Pn(3)−Ga(2)−Ga(3)	96.30(3)	98.25(2)
Pn(1)−Ga(3)−Pn(1)	105.53(5)	105.29(3)	Pn(1)−Ga(3)−Ga(2)	104.45(3)	104.803(19)
Pn(4)−Ga(3)−Pn(1)	111.40(3)	111.401(18)	Pn(4)−Ga(3)−Ga(2)	118.55(3)	118.13(3)
Pn(2)−Ga(4)−Pn(4)	100.97(3)	101.164(18)	Pn(2)−Ga(4)−Ga(4)	118.41(4)	117.97(3)
Pn(4)−Ga(4)−Pn(4)	106.46(5)	106.41(3)	Pn(4)−Ga(4)−Ga(4)	114.12(3)	114.19(2)

A view of a single $[Ga_2Pn_2]^{2-}$ layer is shown in Figure 2. When the structure is viewed along [101], sets of three parallel dumbbells of Ga connected to one another through a set of single, nearly perpendicular dumbbells are apparent. This connectivity results in Ga_2Pn_4 six-membered and Ga_3Pn_2 five-membered rings, as seen when the structure is viewed along [010] (Figures 1 and 3). For the central dumbbell (Ga(4)−Ga(4)) of each parallel set, pairs of gauche Pn atoms are shared with each of six neighboring dumbbells, four of which are the outer parallel dumbbells and two of which are the central parallel dumbbells. The outer parallel dumbbells (Ga(2)−Ga(3)) share pairs of gauche Pn atoms with two central parallel, two outer parallel, and two perpendicular Ga_2Pn_6 moieties. Finally, the perpendicular dumbbells (Ga(1)−Ga(1)) share pairs of gauche Pn atoms with two perpendicular and four outer parallel dumbbells, two from each neighboring set of three parallel dumbbells.

The anions of the structure exhibit uncommon Ga−Ga bonds, which are 2.4048(6), 2.4703(9), and 2.4922(9) Å ($EuGa_2P_2$) and 2.4137(7), 2.4578(10), and 2.4728(10) Å ($EuGa_2As_2$) for Ga(2)−Ga(3), Ga(4)−Ga(4), and Ga(1)−Ga(1), respectively. These distances correspond to approximately twice the covalent radius of Ga ($2r_{Ga}$ = 2.44(4) Å).[31] Ga−Ga dimeric units are known primarily in discrete gallium-halide complexes and in the binary phases GaQ (Q = chalcogen).[32] The $[Ga_2Pn_2]^{2-}$ repeat of the major anion can be viewed as a dimer of a one-electron reduction product of the corresponding GaPn

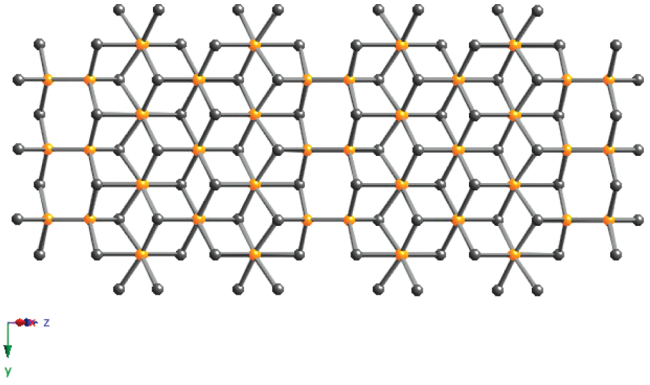

Figure 2. Projection on the (101) plane showing a single $[Ga_2As_2]^{2-}$ layer in $EuGa_2As_2$. Ga and As atoms are shown in gold and gray, respectively.

(31) Cordero, B.; Gómez, V.; Platero-Prats, A. E.; Revés, M.; Echeverría, J.; Cremades, E.; Barragán, F.; Alvarez, S. *Dalton Trans*. **2008**, 2832.

(32) Greenwood, N. N.; Earnshaw, A., Aluminum, Gallium, Indium, and Thallium. In *Chemistry of the Elements*, 2nd ed.; Butterworth-Heinemann: Oxford, U.K., 1997; pp 216−267.

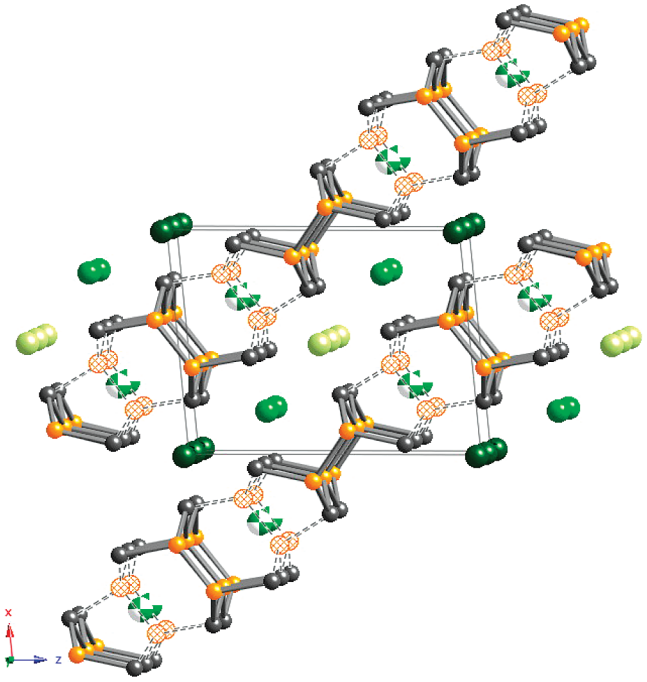

Figure 3. Minor structure postulated from the residual electron density, attributed to the substitution of a Eu atom (white/green spheres) for two Ga atoms (open orange spheres). The dotted lines show bonds in $EuGa_2Pn_2$ that are no longer present after the substitution. Fully occupied Eu sites are shown as solid green spheres; fully occupied Ga sites, solid gold spheres; fully occupied Pn sites, gray spheres.

binary, isoelectronic with GaQ. To date, Ga−Ga dimeric units have been observed in only a few ternary Zintl phases (e.g., $BaGa_2Sb_2$, $Na_2[Ga_3Sb_3]$, $Pr_{12}Ga_4Sb_{23}$, and $Eu_7Ga_6Sb_8$, with Ga−Ga distances from 2.42 to 2.89 Å).[30,33−35] The occurrence of a Ga−Ga bond is thought to reflect a formal Ga oxidation state of +2,[30,32] e.g., for the major structures, $(Eu)^{2+}(Ga_2)^{4+}(Pn_2)^{6-}$. The Ga−Pn distances in the compounds range from 2.4023(12) to 2.4558(13) Å in $EuGa_2P_2$ and from 2.4945(7) to 2.5395(7) Å in $EuGa_2As_2$.

Figure 3 shows how the $EuGa_2Pn_2$ structure can be modified to attain a structure with the stoichiometry $Eu_3Ga_2Pn_4$, surmised from the residual electron density, as described in the experimental crystallography section above. The proposed minor structure contains 4 crystallographically distinct Eu sites and one-dimensional Ga/Pn anionic chains, as shown in Figure 4. Interchangability of a A^{2+} cation with two Ga atoms has also been observed in $A_7Ga_2Sb_6$ (A = Sr, Ba, Eu).[36] Interatomic Eu−Pn distances (including Eu(4P)−Pn distances) range from 2.927(12) to 3.1214(11) Å in $EuGa_2P_2$, and 3.020(17) to 3.220(14) Å in $EuGa_2As_2$. We assume that the minor structure can be incorporated either as randomly distributed units, or as part of an ordered structure in a larger supercell. Our X-ray data do not allow us to clearly distinguish between these possibilities. We note, however, that the occupancies of the minor structures are statistically different in the two compounds. This suggests a random distribution, rather than a superstructure, because a superstructure should result in equal apparent occupancies. A consequence of the presence of the minor structure is that the crystals are more accurately described by the formula $Eu_{1+\delta}Ga_{2-2\delta}Pn_2$, where the refined compositions are $Eu_{1.018}Ga_{1.964}P_2$ and $Eu_{1.014}Ga_{1.985}As_2$. Zintl compounds with strict 1−2−2 stoichiometry are expected to be semiconductors, yet metallic behavior is observed for the $Eu_{1+\delta}Ga_{2-2\delta}Pn_2$ compounds (described below). We suggest that a randomly distributed minority structure as proposed here can give rise to the metallic behavior observed for these phases. However, we also note that metallic behavior was observed for the $EuIn_2Pn_2$ compounds,[8,14] which showed no discernible deviations from 1−2−2 stoichiometry and were also expected to be semiconductors.

Magnetism. $EuGa_2P_2$ and $EuGa_2As_2$ are magnetic due to the rare-earth element cation Eu^{2+} and its f^7 electronic configuration. Magnetic susceptibilities as a function of temperature were measured for single crystals of each compound in an applied field of 0.1 T with the long needle axis, coincident with the *b*-axis direction, oriented either parallel or perpendicular to the applied field (see Figures 5 and 6). The *b*-axis of the unit cell is also the direction of nearest-neighbor europium cations, with Eu−Eu distances of 3.8967(4) and 4.0294(3) Å in $EuGa_2P_2$ and $EuGa_2As_2$, respectively. The Eu−Eu distances in the *ac*-plane are slightly longer than those along the *b*-axis, with shortest distances between Eu cations, Eu(1)−Eu(3) and Eu(1)−Eu(2), of 4.1606(3) and 4.1780(3) Å and 4.2737(3) and 4.2915(3) Å, in $EuGa_2P_2$ and $EuGa_2As_2$, respectively.

The compounds are paramagnetic for temperatures above approximately 30 K and the inverse susceptibility is linear as a function of temperature. A Curie−Weiss fit to the data ($T > 50$ K) indicates ordering temperatures (Weiss constants, θ) of 26 K (P) and 21 K (As), which are in close agreement to observed peaks in the susceptibility at approximately 24 K (P) and 20 K (As). The effective magnetic moments calculated from each fit (8.00 μ_B for (P) and 7.86 μ_B for (As)) correspond well to the theoretical value for a Eu^{2+} ion (7.94 μ_B). Magnetic hysteresis data at 5 K are shown as insets in Figures 5 and 6; they are consistent with ferromagnetic (FM) ordering for $EuGa_2P_2$ and a more complex ordering for $EuGa_2As_2$. For $EuGa_2P_2$, which displays a less-complicated field dependence of the magnetization, the saturation magnetization of 6.3 μ_B is slightly less than the theoretical value for Eu^{2+} ($M^{sat} = 7.0\ \mu_B$).

The magnetization versus field data for $EuGa_2As_2$ indicate several spin reorientations, which are similar in both sample orientations. In both orientations, there is a transition indicated by a change in slope from the low-field regime (approximately ±0.4 T) to a higher-field regime before the compound becomes saturated at approximately 4 T. However, in the perpendicular orientation, this low-field region can be divided further into two

(33) Cordier, G.; Schäfer, H. *Mater. Res. Bull.* **1986**, *21*, 331.
(34) Mills, A. M.; Mar, A. *Inorg. Chem.* **2000**, *39*, 4599.
(35) Park, S.-M.; Kim, S.-J.; Kanatzidis, M. G. *J. Solid State Chem.* **2004**, *177*, 2867.
(36) Xia, S.-Q.; Hullmann, J.; Bobev, S. *J. Sol. State Chem.* **2008**, *181*, 1909.

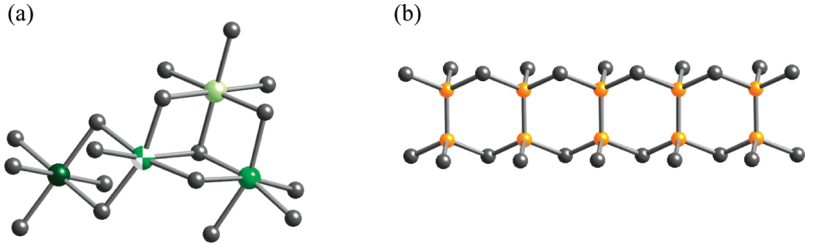

Figure 4. View of (a) the cation coordination and (b) the anion of the minor structure. Atom color scheme is the same as for Figure 3.

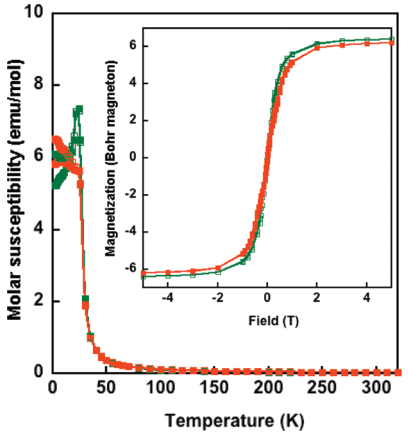

Figure 5. Magnetic susceptibility ($H = 0.1$ T) of $EuGa_2P_2$ as a function of temperature (FC (open symbols) and ZFC (filled symbols) data). Inset shows the hysteresis loop measured at 5 K. Data corresponding to different orientations of the crystal (*b*-axis) relative to the applied field are distinguished by color (*b*-axis parallel, green open symbols; perpendicular, red filled symbols).

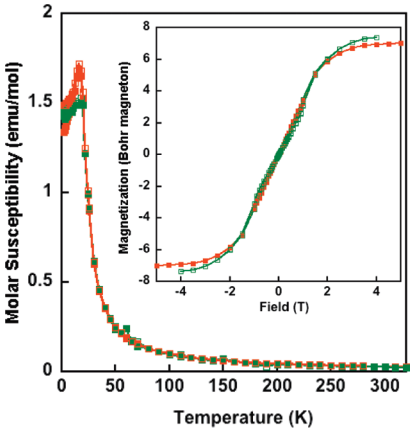

Figure 6. Magnetic susceptibility ($H = 0.1$ T) of $EuGa_2As_2$ as a function of temperature (FC (filled symbols) and ZFC (open symbols) data). Inset shows the hysteresis loop measured at 5 K. Data corresponding to different orientations of the crystal (*b*-axis) relative to the applied field are distinguished by color (*b*-axis parallel, green open symbols; perpendicular, red filled symbols).

gradually increasing, linear regions (±0.1 T and ±0.1 to ± 0.4 T); this may indicate two separate ordering events. Mild hysteretic behavior is also observed in the FM regime, between ±0.4 and ±2 T, typical of a soft ferromagnet. The saturation magnetization is slightly lower with the crystal oriented so that its long needle axis is perpendicular to the applied field. At $H = 4$ T, the saturation magnetization values in the parallel and perpendicular orientations are, respectively, 7.38 and 6.93 μ_B, near those expected for Eu^{2+} (7.0 μ_B).

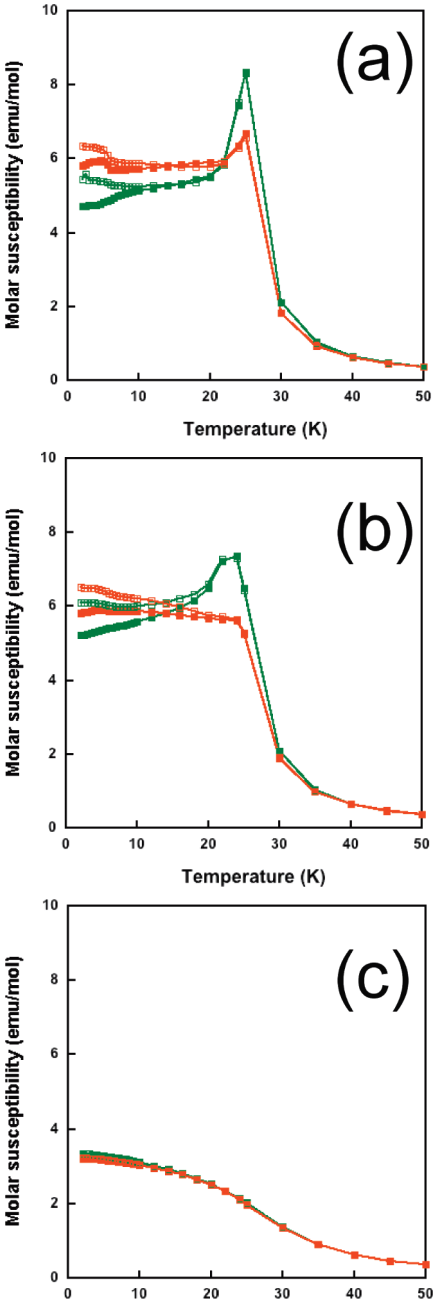

Figure 7. Magnetic susceptibility at $H =$ (a) 0.01 T, (b) 0.1 T, and (c) 1 T of $EuGa_2P_2$ as a function of temperature. Data corresponding to different orientations of the crystal (*b*-axis) relative to the applied field are distinguished by color (*b*-axis parallel, green; perpendicular, red).

Susceptibility versus temperature was additionally measured for the phosphide and arsenide in several applied fields ($H = 0.01$, 0.1, and 1 T (Figures 7 and 8))

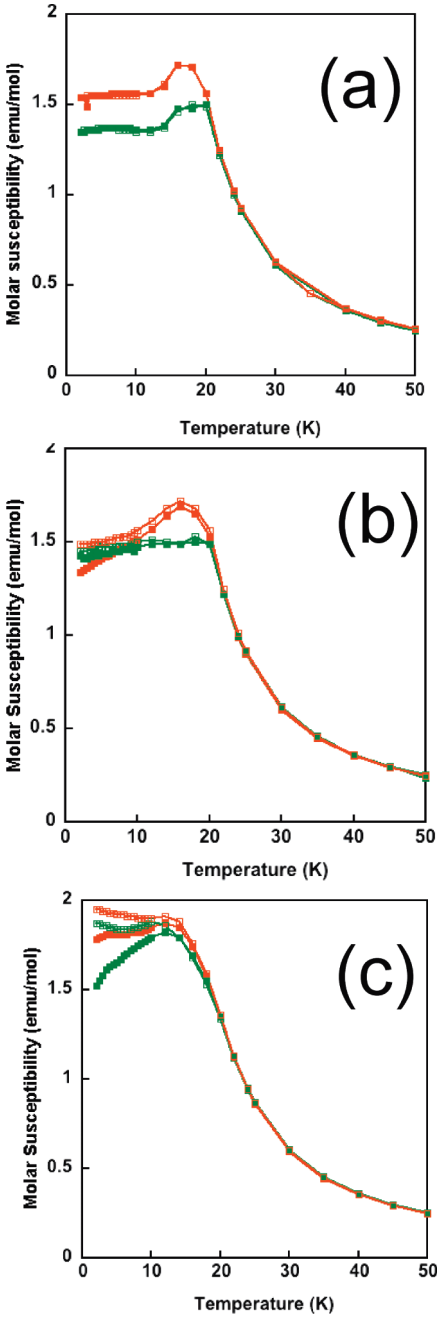

Figure 8. Magnetic susceptibility at H = (a) 0.01 T, (b) 0.1 T, and (c) 1 T of $EuGa_2As_2$ as a function of temperature. Data corresponding to different orientations of the crystal (*b*-axis) relative to the applied field are distinguished by color (*b*-axis parallel, green; perpendicular, red).

with the *b*-axis either parallel or perpendicular to the applied field. At all measured fields, magnetic anisotropy is observed for $EuGa_2P_2$ at temperatures below approximately 40 K, and for $EuGa_2As_2$, at temperatures below approximately 20 K, although for the phosphide the degree of anisotropy in the highest measured field is not as significant as in the arsenide. In the 0.01 T data set, two magnetic transitions are observed for $EuGa_2P_2$: a sharp downturn in the susceptibility at approximately $T = 26$ K in both orientations, indicative of antiferromagnetic (AFM) ordering of the Eu^{2+} cation spins, and a small rise in the susceptibility ($T \approx 6$ K) when the *b*-axis is perpendicular to H, indicative of FM ordering of at least some of the cation spins at lower temperatures. The latter transition appears to be absent in the data acquired in the parallel orientation. For $EuGa_2As_2$ at $H = 0.01$ T, the orientation dependence of the susceptibility is less pronounced. Both orientations show a broad downturn in the susceptibility, centered around $T = 16$ K, characteristic of AFM ordering. It is possible, given the breadth of this transition, that two distinct magnetic transitions are occurring in the arsenide, analogous to the behavior observed for the phosphide, although the two transitions are at closer temperatures in the arsenide. Thus, it can be concluded for both compounds that the crystallographically distinct europium cations may behave as (at least) two distinct, magnetically ordering substructures, which order at different temperatures and in different ways (i.e., FM ordering for some cations in $EuGa_2P_2$, versus all AFM ordered cations in $EuGa_2As_2$. The observation of at least two distinct ordering transitions in the low field data is not unexpected, given that there are at least three crystallographically distinct Eu^{2+} cation sites in the monoclinic crystal structure, and these sites may order independently at different temperatures. With Eu Mössbauer spectroscopy, we have established an analogous behavior for Eu_3InP_3.[37]

Upon increasing the applied field to $H = 0.1$ T, only a single magnetic transition is observed for $EuGa_2P_2$ with the long needle axis oriented perpendicular to the applied magnetic field at $T \approx 26$ K; below this temperature, the magnetization rises monotonically. Similarly, in the same field, only a single magnetic transition is observed for $EuGa_2As_2$ at approximately 20 K, but in the parallel crystal orientation. Below this temperature, the magnetization in this orientation appears saturated. For each compound, in different orientations (parallel for $EuGa_2P_2$, perpendicular for $EuGa_2As_2$), broad downturns in the susceptibility, indicative of AFM ordering, are observed near the highest ordering temperatures observed at lower field; no obvious lower temperature ordering event is observed for either compound. For $EuGa_2As_2$, the AFM transition is observed with the field applied in the direction of the nearest-neighbor europium cations (along [010]). For the phosphide, the AFM transition at 0.1 T must involve coupling of more spatially separated Eu cations in the *ac*-plane. The observed AFM transitions are broad for both compounds, occurring over an approximately 4 K temperature range in the phosphide and an approximately 10 K temperature range in the arsenide. This is suggestive of spin frustration or spin glass behavior. This hypothesis is additionally supported by the divergence of the ZFC/FC curves below the highest temperature ordering events.

Upon further increase of the applied field to 1 T, the divergence in ZFC/FC data is not significant for $EuGa_2P_2$, even though it is more apparent for $EuGa_2As_2$. Furthermore, the downturn in the susceptibility is lost for

(37) Jiang, J.; Payne, A. C.; Olmstead, M. M.; Lee, H.-O.; Klavins, P.; Fisk, Z.; Kauzlarich, S. M.; Hermann, R. P.; Grandjean, F.; Long, G. J. *Inor. Chem.* **2005**, *44*, 2189.

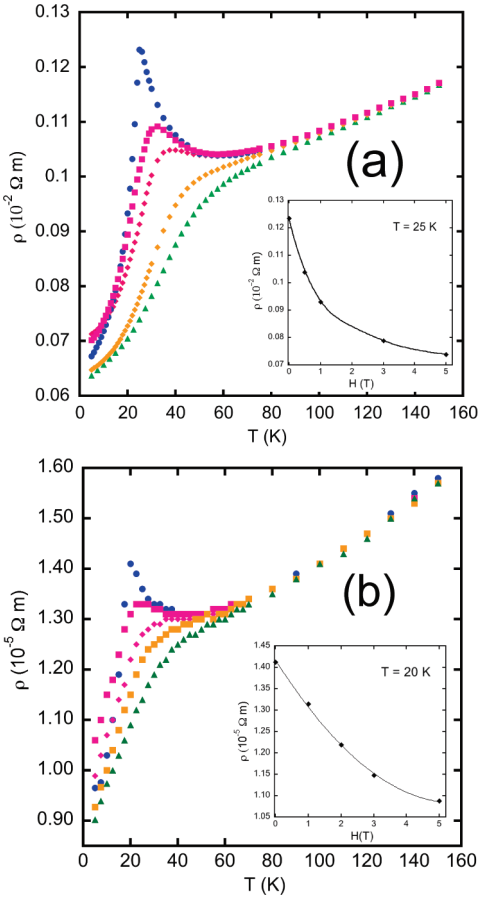

Figure 9. Resistivity as a function of magnetic fields vs temperature measured with the leads attached along the *b*-axis of (a) $EuGa_2P_2$ (with magnetic fields of 0T, blue circles; 0.5T, pink squares; 1T, pink diamonds; 3T, orange squares; and 5T, green triangles) and (b) $EuGa_2As_2$ (with magnetic fields of 0T, blue circles; 1T, pink squares; 2T, pink diamonds; 3T, orange squares; and 5T, green triangles). The insets show resistivity as a function of applied field at the temperatures indicated.

$EuGa_2P_2$, while it is largely retained in $EuGa_2As_2$. The curves for both orientations of the phosphide are suggestive of FM, rather than AFM, ordering at 1 T. For $EuGa_2As_2$ measured at 1 T in both orientations, the broader transition and more discernible ZFC/FC divergence (when compared with the 0.1 T data sets) still suggests a three-dimensional, highly spin-disordered system. Below the broad transition from approximately 20−10 K in $EuGa_2As_2$, the field-cooled susceptibility increases monotonically with decreasing temperature in both orientations, while the ZFC susceptibility in both orientations increases with increasing temperature over the same range. This behavior is consistent with a "frozen," spin-disordered system, suggestive of attempted ferromagnetic ordering of the cation spins for the arsenide. Such ordering is apparently more facile for the phosphide.

Magnetoresistance. Standard four-probe resistivity measurements were made at zero field and several applied fields for the compounds along the *b*-axis. The data are shown in Figure 9. When the compounds are cooled from room temperature in the absence of an applied field, their resistivity decreases with decreasing temperature, consistent with metallic behavior. At 160 K (well above the magnetic ordering temperatures) in zero field, the measured resistivities for $EuGa_2P_2$ and $EuGa_2As_2$ are 1×10^{-3} and 2×10^{-5} Ω m, respectively. The resistivity trend is therefore $EuGa_2P_2 > EuGa_2As_2$, in keeping with the expected trend toward increased metallicity (decreased resistivity) upon descending the periodic table. Over the entire temperature range, the compounds may be classified as metals on the basis of the order of magnitude of their electrical resistivities. However, for the least metallic phase, $EuGa_2P_2$, resistivity values are intermediate between those expected for a semiconductor and for a true metal; $EuGa_2P_2$ may therefore be classified as a poor metal.

Magnetoresistance is not expected for substances having metallic conductivity; typical metals have magnetoresistance of less than 2%, which is due to magnetic field-induced changes in the spin-disorder scattering of the electrical carriers by phonons. However, the title compounds are truly poor metals, or semimetals, which additionally have localized magnetic moments that can affect resistivity in a temperature- and field-dependent fashion, because of magnetic disorder scattering of the conduction electrons by the local moments. For metallic magnets with band structures having valence levels lying near expected metal−insulator transitions, magnetoresistance is frequently observed. Thus it is not surprising that the title compounds exhibit compositionally dependent magnetoresistance, most pronounced near their magnetic ordering temperatures. It is interesting to note that on the basis of the classical definition of a Zintl phase, with each atom in the structure having a closed shell electronic configuration, the compounds are expected to be semiconductors with an energy gap between filled and unfilled levels. However, the present compounds are composed of heavy elements, and thus any observed band gap is expected to be small and/or lie near a compositionally dependent metal−insulator boundary. The slight nonstoichiometry attributed to the minor phase may also have an effect, resulting in metallic properties.

The zero-field resistivity increases near the magnetic ordering transition, at 24 and 20 K for $EuGa_2P_2$ and $EuGa_2As_2$, respectively. The compounds are negative CMR materials, with MR (MR = $[(\rho(H) - \rho(0))/\rho(H)] \times 100\%$) of −80 and −30% for $EuGa_2P_2$ and $EuGa_2As_2$, respectively. Positive MR behavior occurs at lower temperatures and is associated with AF ordering of localized moments, which cause increased carrier scatter (and increased resistivity) upon increasing the applied field. The observation of both positive and negative MR for these compounds is not unexpected from the magnetic data, which show multiple ordering transitions, both FM and AFM, potentially belonging to multiple crystallographically distinct magnetic cation sites.

Conclusion

$EuGa_2P_2$ and $EuGa_2As_2$ represent two new, rare earth-containing Zintl compounds with a new structure type, prepared via flux synthesis. The structure is composed of

shared Ga_2Pn_6 subunits that form an anionic layer interspersed with three crystallographically distinct Eu^{2+} cation sites. There is a small amount of electron density that has been modeled as a minor structure ($\leq 2\%$). Our observations suggest that this minor structure can be accommodated within the main structure, and is randomly distributed in the crystal. The minor structure provides a slight variation in composition and may contribute to the metallic properties observed for these compounds. The tendency for the phosphide is to order ferromagnetically as compared with the arsenide, where there is a greater tendency to order antiferromagnetically. Additionally, there is a significantly more complicated field dependence behavior observed for $EuGa_2As_2$, compared to $EuGa_2P_2$. This difference is attributed to greater coupling strength in the phosphides due to shorter Eu···Eu distances. Both compounds show significant negative magnetoresistive behavior, which is unexpected for metallic compounds such as these. The magnetoresistance decreases from the phosphide (-80%) to the arsenide (-30%). The difference is expected on the basis of the magnetic coupling strength. Comparing the properties of $EuIn_2Pn_2$ and the $EuGa_2Pn_2$ compounds (Pn = P, As), larger Weiss constants, and higher ordering temperatures for the phosphides relative to the arsenides indicate a more favorable exchange energy (lower energetic barrier to coupling). Because communication of the local moment spin alignment occurs through the conduction electron wave function, according to RKKY theory, more tightly coupled local spins will more heavily influence the delocalized carriers, thus leading to greater magnetoresistance. These two new compounds add to the growing number of Zintl phases with unique magnetic and electronic behaviors, which in the present compounds include anisotropic, metallic magnetic behavior and magnetoresistance. Furthermore, the compounds exhibit exotic magnetic and electronic behavior in being magnetoresistive metals, as do many other AM_2X_2 compounds, suggesting that this composition may somehow give rise to atypical magnetic and electronic behavior.

Acknowledgment. We thank James Fettinger, Christine Beavers, and Marilyn Olmstead for useful discussion. This work was supported by the National Science Foundation (Grants DMR-0600742 and DMR-085478). A.M.G. acknowledges a Career Award at the Scientific Interface from the Burroughs Wellcome Fund (Award 1007294) for support.

Supporting Information Available: X-ray crystallographic data in CIF format for the single-crystal refinements of $EuGa_2P_2$ and $EuGa_2As_2$. This material is available free of charge via the Internet at http://pubs.acs.org.